Site-selective spectroscopy of Tm^{3+} centers in CaF_2:Tm^{3+}

Nicholas M. Strickland* and Glynn D. Jones
Department of Physics and Astronomy, University of Canterbury, PB 4800, Christchurch, New Zealand
(Received 14 May 1997)

By polarized laser selective excitation, two single Tm^{3+} ion centers of tetragonal (C_{4v}) and trigonal (C_{3v}) symmetry have been identified in CaF_2:0.05%Tm^{3+}. Both of these centers exhibit blue, violet, and ultraviolet upconversion fluorescence under red-dye laser excitation. Crystal-field analyses of their assigned energy levels and fluorescence lifetime data are presented. By Zeeman infrared-absorption spectroscopy, a further Tm^{3+} center of cubic symmetry is identified. Measurement of the line strength of its single infrared-absorption line provides a direct method of determining relative Tm^{3+} center concentrations. With deuteration treatment, two families of D^- centers derived from the C_{4v} and C_{3v} centers appear. Energy levels for four of the D^--modified C_{4v} centers are reported. [S0163-1829(97)00841-2]

I. INTRODUCTION

We report the results of a laser selective excitation (LSE) study of CaF_2:0.05% Tm^{3+}. At Tm^{3+} concentrations of 0.05% or less, single Tm^{3+} ion centers are the major centers present. From the polarized LSE spectra, we identify a principal center of C_{4v} symmetry and a center of C_{3v} symmetry. A further Tm^{3+} center of cubic symmetry is identified through Zeeman studies of its single infrared-absorption line.

In the cubic CaF_2 crystal lattice, lower than cubic-symmetry rare-earth centers are formed by charge compensation of the trivalent rare-earth ion by nearby interstitial F^- ions. As such centers can be oriented along equivalent crystal axes, no net polarization dependence will appear in their absorption spectra. However, previous studies of rare-earth-doped CaF_2 have shown that a polarization dependence can be detected by LSE.[1–4] This is because differently oriented centers are preferentially excited with a polarized laser beam to produce polarized emission. This polarization dependence is used here to determine the Tm^{3+} point symmetries for two Tm^{3+} centers studied by LSE and to assign irreducible representation labels for the crystal-field levels of the C_{4v} center.

Both of these centers produced upconversion fluorescence when pumped at laser frequencies corresponding to excited-state absorption (ESA) transitions. Two sets of ESA transitions, $^3F_4 \rightarrow {}^1G_4$ and $^3H_4 \rightarrow {}^1D_2$, pumped in the 650 nm region, produced blue, violet, and ultraviolet upconversion fluorescence. A preliminary report of the upconversion fluorescence for the C_{4v} center has been given in an earlier brief account.[5]

Because a Tm^{3+} cubic-symmetry center is centrosymmetric, electric-dipole transitions between $4f^{12}$ electronic states are strictly forbidden, and only magnetic-dipole transitions can be observed. For absorption transitions from the $^3H_6$ ground multiplet, the magnetic-dipole selection rules of $\Delta L = \Delta S = 0$, $\Delta J = 0, \pm 1$ allow magnetic-dipole transitions only to the $^3H_5$ multiplet. One strong transition in the absorption spectrum of the $^3H_5$ multiplet region has been assigned to a Tm^{3+} cubic center on the basis of its splitting pattern in applied magnetic fields.

II. EXPERIMENTAL TECHNIQUES

The CaF_2 crystals containing 0.01–0.05 % Tm^{3+} were grown by the Bridgeman-Stockbarger method in graphite crucibles in a 38 kW Arthur D. Little rf induction furnace. Starting materials were CaF_2 crystal offcuts purchased from Optovac Inc. and 99.9% pure TmF_3 purchased from Alpha Inorganics Inc. Crystal boules were grown in a vacuum of 10^{-5} torr at a lowering rate of 8 mm h^{-1} and oriented by reference to intersecting $\langle 111 \rangle$ cleavage planes. Deuteride (D^-) ions could be diffused into the crystals by heating the crystal samples to 850 °C in $\frac{2}{3}$ atmosphere of deuterium gas and in contact with molten aluminum for periods of up to 40 h.

Optical absorption spectra were recorded photoelectrically with a Spex 1701 0.75 m monochromator using EMI 9558 or 6255 photomultiplier tubes and processed by a voltage-to-frequency converter. The radiation source was a voltage-stabilized 100 W tungsten-halogen lamp. Infrared-absorption spectra over the range 4000–10 000 cm^{-1} were recorded on a BioRad FTS-40 Fourier transform spectrometer at 0.25 cm^{-1} resolution using a tungsten-halogen source, quartz beam splitter, and indium-antimonide detector.

The laser excitation experiments were performed using either a Spectra-Physics 375 cw dye laser pumped by a Spectra-Physics 2045E argon-ion laser or a Coherent 899 cw Ti:sapphire laser pumped by a Coherent I-90 argon-ion laser. The resulting fluorescence was analyzed by a Spex 1403 monochromator equipped with a RCA C31034 photomultiplier and using photon-counting techniques. Fluorescence lifetimes were measured using a PRA LN107 dye laser pumped by a PRA LN1000 nitrogen laser. The fluorescence signal was collected by the Spex 1701 monochrometer, equipped with an EMI 9558 photomultiplier tube, and recorded on a digital storage oscilloscope.

Rhodamine 640 and coumarin 460 laser dyes were used to pump the $^3F_3$, $^3F_2$, and $^1G_4$ multiplets of Tm^{3+}. The rhodamine 640 laser dye was also used to obtain upconversion-fluorescence by pumping $^3F_4 \rightarrow {}^1G_4$ and $^3H_4 \rightarrow {}^1D_2$ excited-state absorption transitions. The lifetime of the $^1D_2$ multiplet was obtained by using both lasers simultaneously, with the cw laser pumping $^3H_6 \rightarrow {}^3F_3$ absorp-

TABLE I. Energies (in cm^{-1}) and wave function composition of the intermediate coupled multiplets of Tm^{3+}, as derived from the C_{4v} center data.

Multiplet	Barycenter	Intermediate-coupled wave function
$^3H_6(Z)$	400	$0.9957\|^3H_6\rangle+0.0921\|^1I_6\rangle$
$^3F_4(Y)$	6000	$0.7954\|^3F_4\rangle+0.5374\|^1G_4\rangle-0.2804\|^3H_4\rangle$
$^3H_5(X)$	8600	$1.0000\|^3H_5\rangle$
$^3H_4(A)$	12900	$0.7739\|^3H_4\rangle+.5185\|^3F_4\rangle-0.3636\|^1G_4\rangle$
$^3F_3(B)$	14700	$1.0000\|^3F_3\rangle$
$^3F_2(C)$	15300	$0.8780\|^3F_2\rangle-0.4579\|^1D_2\rangle-0.1395\|^3P_2\rangle$
$^1G_4(D)$	21500	$0.7609\|^1G_4\rangle+0.5678\|^3H_4\rangle-0.3140\|^3F_4\rangle$
$^1D_2(E)$	28200	$0.6381\|^1D_2\rangle+0.6361\|^3P_2\rangle+0.4338\|^3F_2\rangle$
$^1I_6$	35200	$0.9957\|^1I_6\rangle-0.0921\|^3H_6\rangle$
$^3P_0$	35700	$0.9692\|^3P_0\rangle-0.2462\|^1S_0\rangle$
$^3P_1$	36600	$1.0000\|^3P_1\rangle$
$^3P_2$	38400	$0.7589\|^3P_2\rangle-0.6190\|^1D_2\rangle-0.2023\|^3F_2\rangle$
$^1S_0$	75000	$0.9692\|^1S_0\rangle+0.2462\|^3P_0\rangle$

tion transitions and the pulsed laser pumping $^3H_4\rightarrow{}^1D_2$ excited-state absorption transitions.

All the above absorption and laser excitation experiments were performed with the crystal samples cooled by a CTI Cryogenics Cryodyne 22C closed-cycle helium cryostat. The sample temperature could be varied between 10 K and room temperature.

The infrared Zeeman measurements employed a cryostat with an Oxford Instruments 4 T superconducting solenoid built into its helium can. The crystals were mounted in a central tube through the solenoid. This arrangement eliminated the need for low-temperature infrared windows and gave crystal temperatures of 10 K. All the Zeeman spectra were recorded for the infrared radiation beam along the magnetic field direction.

III. SPECTROSCOPY OF CaF_2:Tm^{3+}

The $4f^{12}$ lowest-energy configuration appropriate to Tm^{3+} has a total of 91 electronic states in 13 free-ion multiplets. Multiplets are labeled either by the leading $^{2S+1}L_J$ term in the intermediate coupled free-ion wave function or by the single letter notation indicated in Table I. The crystal-field levels of a given multiplet are denoted by both the appropriate letter for that multiplet and by a numerical subscript, in sequence from the lowest-energy level of the multiplet. The free-ion multiplet wave functions and barycenters, obtained from the calculations of Sec. III C are given in Table I.

Absorption spectra of the first seven excited multiplets of CaF_2:Tm^{3+} are presented in Fig. 1. The spectra of infrared absorption transitions to the $^3F_4$ and $^3H_5$ multiplets were recorded for a 30 mm boule of CaF_2:0.01%Tm^{3+}. The optical spectra were recorded for a 2 mm thickness of CaF_2:0.05%Tm^{3+}. Transitions associated with three centers, labeled A, B, and O have been so identified in Fig. 1. These centers are structurally identical to three centers previously assigned for CaF_2:Er^{3+}:[6–9] (1) a tetragonal (C_{4v}) symmetry center, the A center, with the charge compensating F^- ion in the $\langle 100\rangle$ nearest-neighbor interstitial position, (2) a trigonal (C_{3v}) symmetry center, the B center, in which the charge-compensating F^- ion was proposed to be in the $\langle 111\rangle$ next-nearest-neighbor interstitial position (this B center was later shown to have a more complex trigonal configuration[1]), and (3) a center with cubic (O_h) symmetry, having remote F^- charge compensation.

For the non-Kramers ions such as Tm^{3+}, the electric-dipole selection rules for C_{4v} and for C_{3v} symmetry significantly restrict the number of transitions that can be observed. The absence of many transitions makes spectral assignments more difficult.

Laser selective excitation is a powerful method for resolving lines of multicenter spectra. A tunable dye laser is used selectively to excite a particular absorption line of a given center and the resulting fluorescence monitored. As only the selected center is excited, the resulting fluorescence arises from this center alone.[1–4,6] By this technique, excitation and fluorescence spectra can be obtained for each center exclusively in turn. Excitation and fluorescence spectra for two single Tm^{3+} centers were measured for CaF_2:0.05%Tm^{3+} and these centers are determined to have Tm^{3+} ions in sites of C_{4v} and C_{3v} symmetry.

A. Laser selective excitation: C_{4v} center

The transition polarizations for the C_{4v} center were determined by appropriate choices of polarizations for the incident laser and for the detected fluorescence. The chosen axes have the laser beam incident along the x axis and the fluorescence monitored in the z direction. The polarization of the laser is thus set at either y or z and a polarization analyzer is introduced before the spectrometer to admit either the x- or y-polarized component of the fluorescence. The standard notation for this experimental configuration is $x(ab)z$ where x indicates the laser propagation direction and z the fluorescence detection direction. $a=y$ or z and $b=x$ or y indicate the choice of laser polarization and fluorescence analyzer polarization, respectively. Since only the polarizations are changed, the x and z propagation directions are omitted in the labeling of Figs. 2 and 3. For C_{4v} centers in a CaF_2 crystal oriented with its principal axes parallel to the chosen x,y,z axes, the relative intensities of detected fluorescence for each combination of laser and fluorescence polarization are summarized in Table II. From the measured polarization, possible irrep combinations can be determined from the selection rules of Table III.

Figures 2(a)–2(d) show the excitation spectra of the $^3H_4(A)$, $^3F_3(B)$, $^3F_2(C)$, and $^1G_4(D)$ multiplets obtained by tuning the laser continuously through the region of the absorption transitions to each of these multiplets while monitoring a single appropriate fluorescence transition. Figures 2(e) and 2(f) are upconversion excitation spectra obtained by tuning the laser through the $^3F_4(Y)\rightarrow{}^1G_4(D)$ and $^3H_4(A)\rightarrow{}^1D_2(E)$ excited-state absorption (ESA) transitions. Fluorescence spectra, obtained by setting the laser to pump a strong isolated absorption line and scanning the spectrometer through the region of the fluorescence transitions, are shown in Fig. 3.

In order to obtain energy-level irreducible representations from these spectra, we need the decomposition of J multiplets, transforming as irreducible representation of the full-

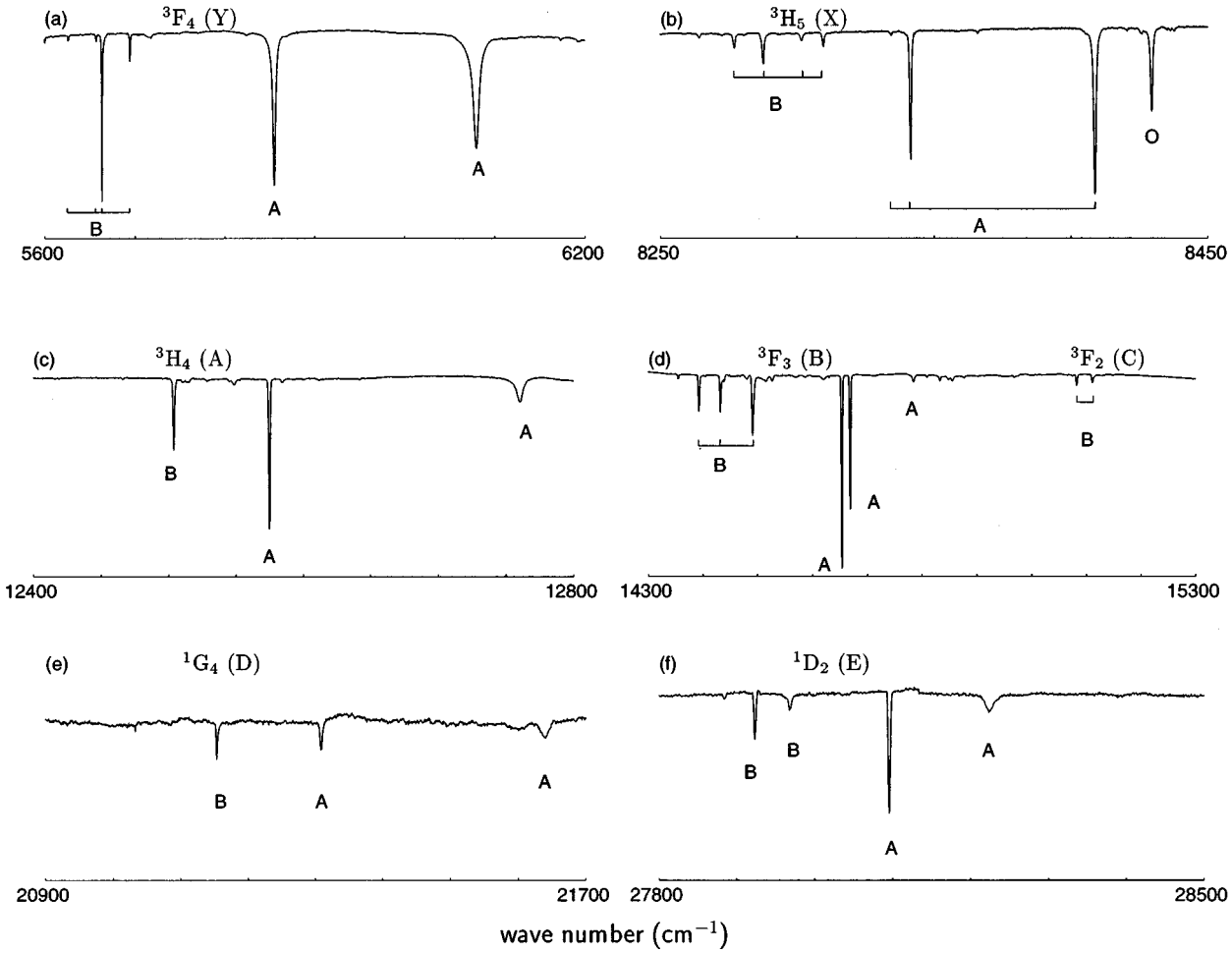

FIG. 1. 10 K absorption spectra of transitions to the (a) $^3F_4$, (b) $^3H_5$, (c) $^3H_4$, (d) $^3F_3$ and $^3F_2$, (e) $^1G_4$, and (f) $^1D_2$ multiplets of CaF_2:Tm^{3+}. Spectra (a) and (b) were recorded for a 30 mm thickness of CaF_2:0.01%Tm^{3+}, and spectra (c)–(f) for a 2 mm thickness of CaF_2:0.05%Tm^{3+}. Assigned absorption transitions are labeled *A* (C_{4v} center), *B* (C_{3v} center) and *O* (cubic center).

TABLE II. Polarization ratios for C_{4v} centers in ⟨100⟩-oriented CaF_2 crystals.

Transition polarizations		Polarization geometry			
Absorption	Emission	*yx*	*yy*	*zx*	*zy*
π	π	0	1	0	0
	σ	1	0	1	1
	π_{md}	1	0	0	0
	σ_{md}	0	1	1	1
π_{md}	π	0	0	0	1
	σ	1	1	1	0
	π_{md}	0	0	1	0
	σ_{md}	1	1	0	1
σ	π	1	0	1	1
	σ	1	2	1	1
	π_{md}	0	1	1	1
	σ_{md}	2	1	1	1
σ_{md}	π	1	1	1	0
	σ	1	1	1	2
	π_{md}	1	1	0	1
	σ_{md}	1	1	2	1

rotation group, into the point-group irreps.[10] The $^3F_3$ excitation spectrum, Fig. 2(b), shows that the transitions from the ground state to this multiplet are σ, π, π_{md}, and σ allowed, respectively. As the $J=3$ multiplet decomposes as $\gamma_2+\gamma_3+\gamma_4+2\gamma_5$ irreducible representations of C_{4v}, the selection rules of Table II are only consistent with the ground state being either a γ_3 or γ_4 level. Further distinction is not possible purely on the basis of LSE experiments. It is necessary to appeal to crystal-field calculations to determine to which of these irreducible representations the ground-state level belongs. If crystal-field parameters similar to those obtained for other C_{4v} centers of CaF_2 are adopted, the ground

TABLE III. Polarization selection rules for C_{4v} symmetry. σ indicates transitions which are both electric and magnetic dipole σ allowed.

	γ_1	γ_2	γ_3	γ_4	γ_5
γ_1	π	π_{md}			σ
γ_2	π_{md}	π			σ
γ_3			π	π_{md}	σ
γ_4			π_{md}	π	σ
γ_5	σ	σ	σ	σ	π, π_{md}

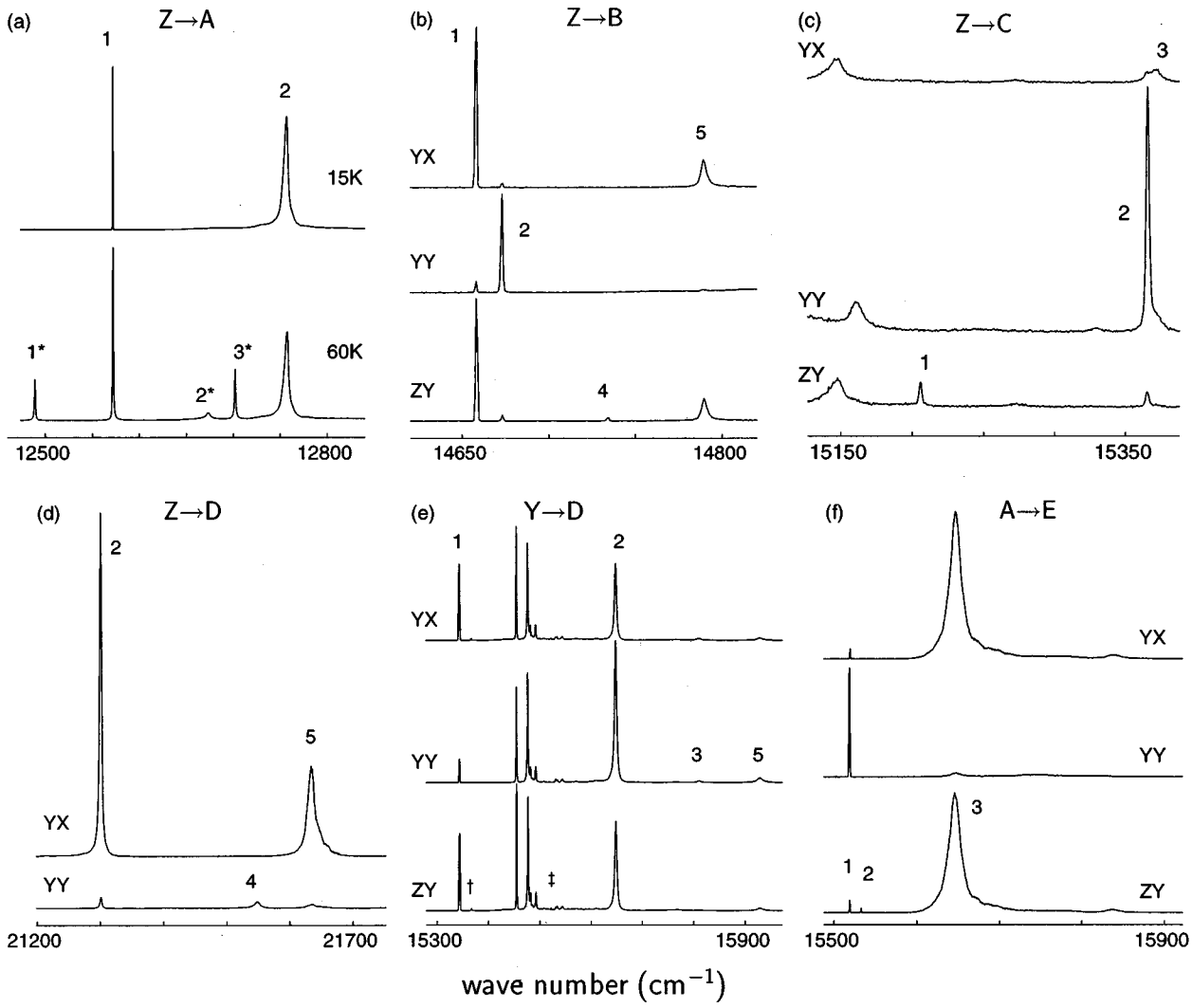

FIG. 2. 15 K (unless indicated) excitation spectra of the $C_{4v}(A)$ center in CaF_2:0.05%Tm^{3+}. (a) $Z \rightarrow A$ transitions at 15 K and 60 K, monitoring $A_1 \rightarrow Z_2$ (σ) at 12 488 cm^{-1}, (b) polarized $Z \rightarrow B$ transitions, monitoring $A_1 \rightarrow Z_1$ (π) at 12 572 cm^{-1}, (c) polarized $Z \rightarrow C$ transitions, monitoring $A_1 \rightarrow Z_1$ (π) at 12 572 cm^{-1}, (d) polarized $Z \rightarrow D$ transitions, monitoring $D_1 \rightarrow Y_1$ (π) at 15 345 cm^{-1}, (e) polarized $Y \rightarrow D$ ESA transitions, monitoring $D_1 \rightarrow Z_2$ (σ) at 20 918 cm^{-1}, (f) polarized $A \rightarrow E$ ESA transitions, monitoring $E_1 \rightarrow B_2$ (σ) at 13 415 cm^{-1}. Excitation transitions are labeled by numerical labels for energy levels of the upper multiplet, with transitions originating from the first excited state of the lower multiplet denoted by *. In spectrum (e), the group of unlabeled lines between 15 450 and 15 550 cm^{-1} are due to cross pumping of other Tm^{3+} centers, while the lines labeled † and ‡ are the $Z_1 \rightarrow C_2$ GSA and $A_1 \rightarrow E_1$ ESA transitions, respectively.

state is unequivocally a γ_3 state.[11] This would then determine the levels of the $^3F_3$ multiplet observed by absorption to be γ_5, γ_3, γ_4, and γ_5, respectively, with the one remaining γ_2 level having a forbidden absorption transition from the ground state.

From this starting point, the remaining experimental levels and irreducible representation listed in Table IV can be determined from the polarization dependence and temperature dependence of the excitation and fluorescence spectra of Figs. 2 and 3. Transitions from excited states of a multiplet increase in intensity with increasing temperature. Spectral hole-burning experiments[12] have shown that the Z_1 and A_1 states of this center were singlet states of the same C_{4v} irreducible representation, in agreement with the assignments made here. In Table IV the experimentally determined levels are compared with the results of a crystal-field fit, discussed in Sec. III C.

With only one exception, all of the single-laser upconversion-excitation transitions observed for this center arose from pumping ESA transitions. The one ground-state absorption (GSA) transition which produced upconversion fluorescence is the $Z_1 \rightarrow C_2$ transition, indicated by † in Fig. 2(e). This spectrum, which shows predominantly $^3F_4(Y) \rightarrow {}^1G_4(D)$ ESA transitions, includes many strong lines which are not associated with the C_{4v} center, but rather are from overlap of fluorescence transitions corresponding to other centers. These other centers, only seen weakly in the absorption spectra, are thought to be cluster centers which have higher upconversion efficiencies than the single-ion centers, because of efficient energy transfer between ions. Transitions which are associated with the C_{4v} center could be distinguished from these by their reduction in intensity when the spectrometer was detuned slightly (~ 1 cm^{-1})

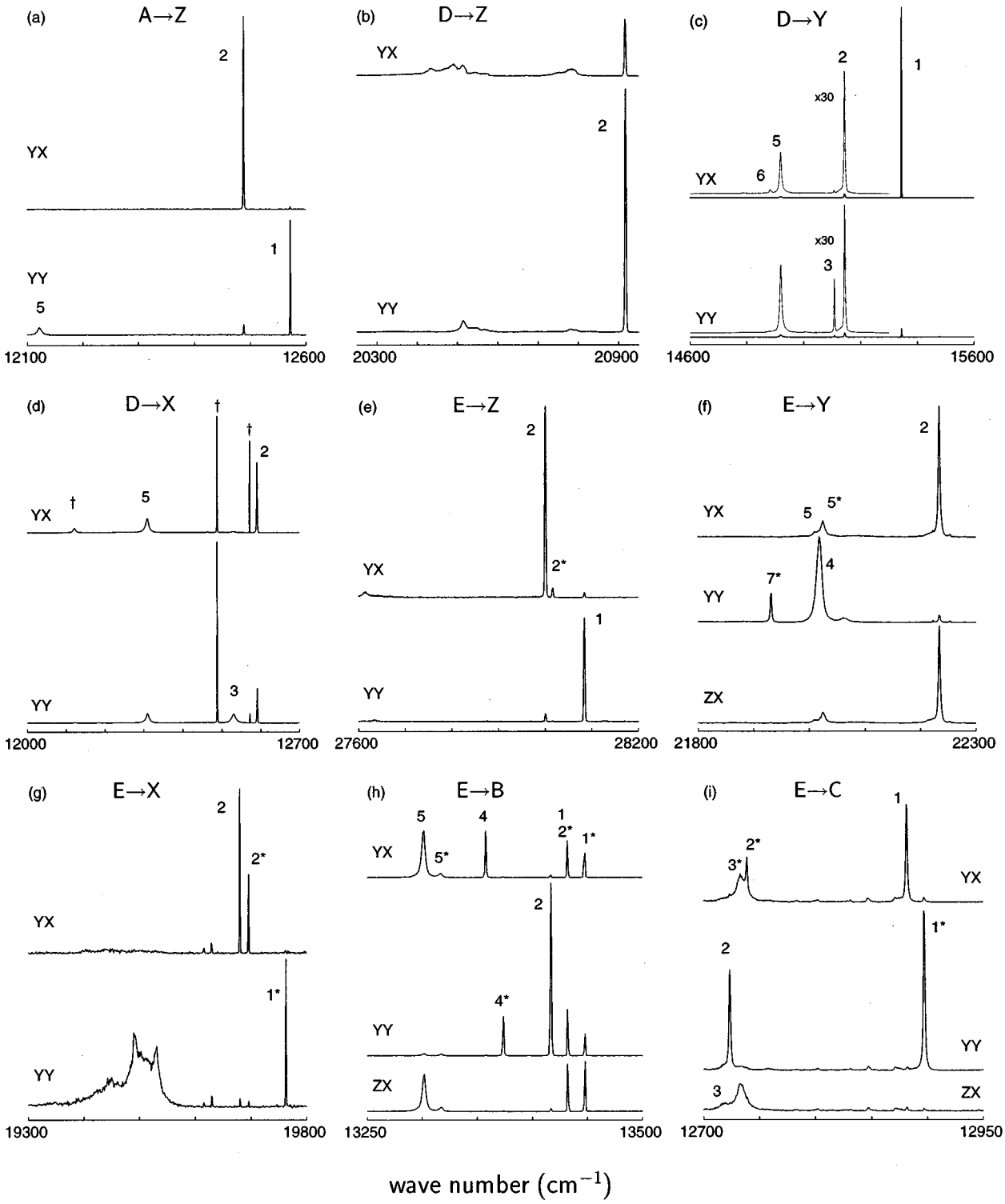

FIG. 3. 15 K fluorescence spectra of the $C_{4v}(A)$ center in CaF_2:0.05%Tm^{3+}. (a) Polarized $A \rightarrow Z$ transitions, pumping $Z_1 \rightarrow B_2$ (π) at 14 675 cm^{-1}, (b), (c), (d) polarized $D \rightarrow Z$, $D \rightarrow Y$, and $D \rightarrow X$ transitions, pumping $Z_1 \rightarrow D_2$ (σ) at 21 302 cm^{-1}, (e), (f), (g), (h), (i) polarized $E \rightarrow Z$, $E \rightarrow Y$, $E \rightarrow X$, $E \rightarrow B$, and $E \rightarrow C$ transitions, pumping $A_1 \rightarrow E_1$ (π) ESA at 15 518 cm^{-1}. Fluorescence transitions are labeled by numerical labels for energy levels of the lower multiplet, with transitions originating from the first excited state of the upper multiplet denoted by *.

from the peak of the fluorescence transition being monitored. Transitions associated with other centers remain unchanged in intensity. The two transitions labeled with † and ‡ were shown by this process, and by their polarization behavior, to be associated with the C_{4v} center, despite not matching any $^3F_4 \rightarrow {}^1G_4$ transitions. The transition labeled with † corresponds in energy to the $Z_1 \rightarrow C_2$ transition and the transition labeled with ‡ corresponds to the $A_1 \rightarrow E_1$ ESA transition. The weakness of this latter line in the $^3F_4 \rightarrow {}^1G_4$ spectrum is attributed to a low $^1D_2 \rightarrow {}^1G_4$ branching ratio.

TABLE IV. Measured and calculated crystal-field energy levels for the CaF_2:Tm^{3+} C_{4v} center.

Energy level		Energies (cm^{-1})	
		measured	calculated
$^3H_6$	γ_3	0	5.6
	γ_5	84.0	94.3
	γ_1	-	236.9
	γ_4	-	402.2
	γ_3	-	465.9
	γ_2	-	488.9
	γ_5	-	496.7
	γ_4	-	555.9
	γ_1	-	562.7
	γ_5	-	690.0
$^3F_4$	γ_1	5658.0	5646.5
	γ_5	5857.4	5853.4
	γ_2	5893.9	5901.9
	γ_3	6069.7	6070.5
	γ_5	6082.1	6077.5
	γ_1	6118.1	6119.7
	γ_4	6173.1	6171.9
$^3H_5$	γ_4	8342.2	8337.9
	γ_5	8411.7	8408.1
	γ_2	8472.1	8472.0
	γ_3	-	8636.8
	γ_5	8694.1	8673.6
	γ_5	-	8697.4
	γ_1	-	8762.7
	γ_2	-	8780.9
$^3H_4$	γ_3	12571.9	12577.9
	γ_5	12757.2	12763.9
	γ_1	-	12804.7
	γ_2	-	12903.3
	γ_4	-	12984.8
	γ_1	-	13035.1
	γ_5	-	13095.8
$^3F_3$	γ_5	14659.4	14663.2
	γ_3	14674.7	14677.1
	γ_2	14720.9	14725.3
	γ_4	14732.7	14726.3
	γ_5	14789.3	14790.6
$^3F_2$	γ_4	15206	15213.5
	γ_3	15365	15364.4
	γ_5	15370	15368.6
	γ_1	-	15448.8
$^1G_4$	γ_1	21002.1	20995.0
	γ_5	21302.4	21300.3
	γ_2	21491.5	21498.9
	γ_3	21549.4	21549.3
	γ_5	21633.6	21638.4
	γ_4	-	21722.3
	γ_1	-	21730.8
$^1D_2$	γ_3	28089.8	28075.9
	γ_4	28105.7	28112.4
	γ_5	28218.1	28222.3
	γ_1	-	28253.4

TABLE V. Polarization selection rules for C_{3v} symmetry. σ indicates transitions which are both electric and magnetic dipole σ allowed.

	γ_1	γ_2	γ_3
γ_1	π	π_{md}	σ
γ_2	π_{md}	π	σ
γ_3	σ	σ	π, π_{md}, σ

B. Laser selective excitation: C_{3v} center

While many energy levels of the trigonal-symmetry C_{3v} center can be determined from the LSE experiments, the polarization ratios are not as straightforward to interpret as those of the C_{4v} center.

The transition selection rules for C_{3v} symmetry are summarized in Table V, with the mixed (σ,π) polarization of $\gamma_3 \rightarrow \gamma_3$ transitions leading to arbitrary polarization ratios whenever such transitions are involved. For CaF_2 crystals oriented with their $\langle 100 \rangle$ crystal axes parallel to the z and x axes, C_{3v} centers are expected to have yx:yy:zx:zy polarization ratios of unity for all transitions, because of the equal inclination of all possible orientations of the C_{3v} center to the z and x axes. Well-defined C_{3v} polarization ratios do result for crystals oriented with their $\langle 111 \rangle$ body-diagonal axis aligned parallel with the z (fluorescence-detection) axis, and these are summarized in Table VI. These predicted polarization ratios are closer to 1:1 compared to those found for C_{4v} centers, as there are four possible nonorthogonal orientations of C_{3v} centers.

The absence of any polarization dependence for $\langle 100 \rangle$-oriented crystals and the polarization dependences observed for $\langle 111 \rangle$-oriented crystals confirm the C_{3v} symmetry of this center. However, the closeness of the various polarization ratios to 1:1 can lead to ambiguities in the interpretation of polarization data. Definite assignment of irreducible repre-

TABLE VI. Polarization ratios for C_{3v} centers in $\langle 111 \rangle$-oriented CaF_2 crystals.

Transition polarizations		Polarization geometry			
Absorption	Emission	yx	yy	zx	zy
π	π	2	6	1	1
	σ	7	3	8	8
	π_{md}	6	2	1	1
	σ_{md}	3	7	8	8
π_{md}	π	1	1	2	6
	σ	8	8	7	3
	π_{md}	1	1	6	2
	σ_{md}	8	8	3	7
σ	π	7	3	8	8
	σ	11	15	10	10
	π_{md}	3	7	8	8
	σ_{md}	15	11	10	10
σ_{md}	π	8	8	7	3
	σ	10	10	11	15
	π_{md}	8	8	3	7
	σ_{md}	10	10	15	11

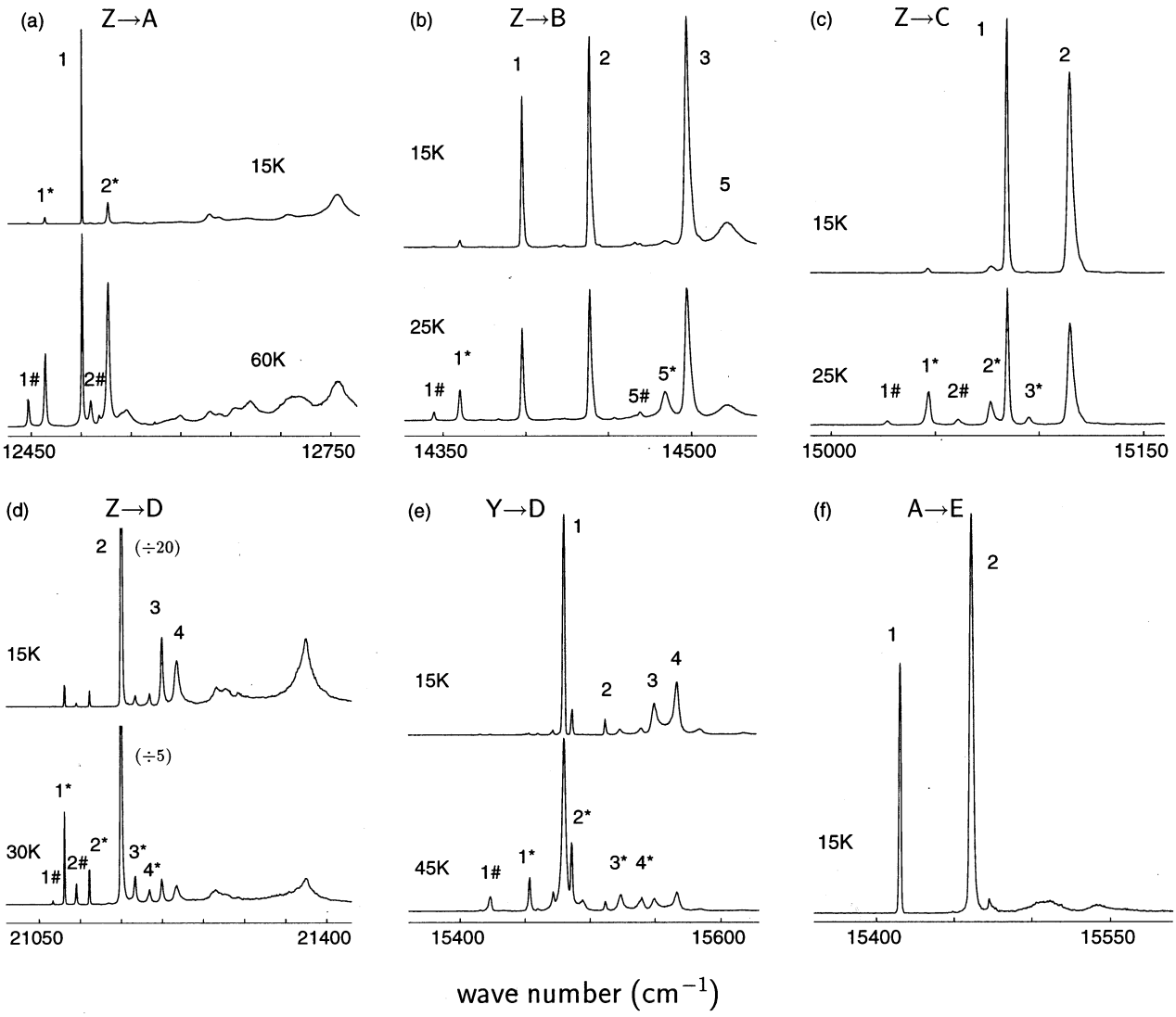

FIG. 4. Excitation spectra of the $C_{3v}(B)$ center in CaF_2:0.05%Tm^{3+}. (a) $Z \rightarrow A$ transitions at 15 K and 60 K, monitoring $A_1 \rightarrow Z_3$ at 12 448 cm^{-1}, (b) $Z \rightarrow B$ transitions at 15 K and 25 K, monitoring $A_1 \rightarrow Z_1$ at 12 502 cm^{-1}, (c) $Z \rightarrow C$ transitions at 15 K and 25 K, monitoring $A_1 \rightarrow Z_1$ at 12 502 cm^{-1}, (d) $Z \rightarrow D$ transitions at 15 K and 30 K, monitoring $D_1 \rightarrow Y_1$ at 15 479 cm^{-1}, (e) $Y \rightarrow D$ ESA transitions at 15 K and 45 K, monitoring $D_1 \rightarrow Z_2$ at 21 082 cm^{-1}, (f) $A \rightarrow E$ ESA transitions at 15 K, monitoring $E_1 \rightarrow Y_2$ at 22 254 cm^{-1}. Excitation transitions are labeled by numerical labels for energy levels of the upper multiplet, with transitions originating from the first and second excited states of the lower multiplet denoted with $*$ and #, respectively.

sentation to energy levels has not been possible using these polarization ratio data. For this reason, polarized spectra are not presented for this center. Temperature-dependent spectra are displayed in some cases and these aided in the determination of energy levels.

Figures 4(a)–4(d) show the excitation spectra of the $^3H_4(A)$, $^3F_3(B)$, $^3F_2(C)$, and $^1G_4(D)$ multiplets while Figs. 4(e) and 4(f) are ESA upconversion excitation spectra. The fluorescence spectra are shown in Fig. 5.

The experimental energy levels of Table VII (without irreducible representation assignments) have been deduced from the LSE data. The experimentally determined levels are compared with the results of a crystal-field fit, as discussed in Sec. III C.

Some anomalous features appear in the spectra. In the $^1D_2(E) \rightarrow {}^3F_4(Y)$ fluorescence spectrum, Fig. 5, seven transitions appear. Only six levels are expected for the $^3F_4(Y)$ multiplet, and those transitions which have been labeled are consistent with the $^1G_4(D) \rightarrow {}^3F_4(Y)$ fluorescence spectrum, Fig. 5(c). The extra transition, near 22 110 cm^{-1}, appears to tune with the C_{3v} center but remains unassigned. Another unassigned transition appears at 19 801 cm^{-1} in the $^1D_2(E) \rightarrow {}^3H_5(X)$ fluorescence spectrum, Fig. 5(g). The transition from the D_1 level to this $^3H_5$ level should be present in the $^1G_4(D) \rightarrow {}^3H_5(X)$ spectrum, Fig. 5(d), but is not observed. In addition, the crystal-field splitting between this level and the other $^3H_5$ levels would be anomalously large in comparison to the other multiplets of this center, and also to the calculated splitting. The crystal-field fit described in Sec. III C was repeated, omitting the experimental energies of the $^3H_5$ multiplet, and gave no indication that such a large splitting would be expected. Hence the line at 19 801 cm^{-1} also remains unassigned.

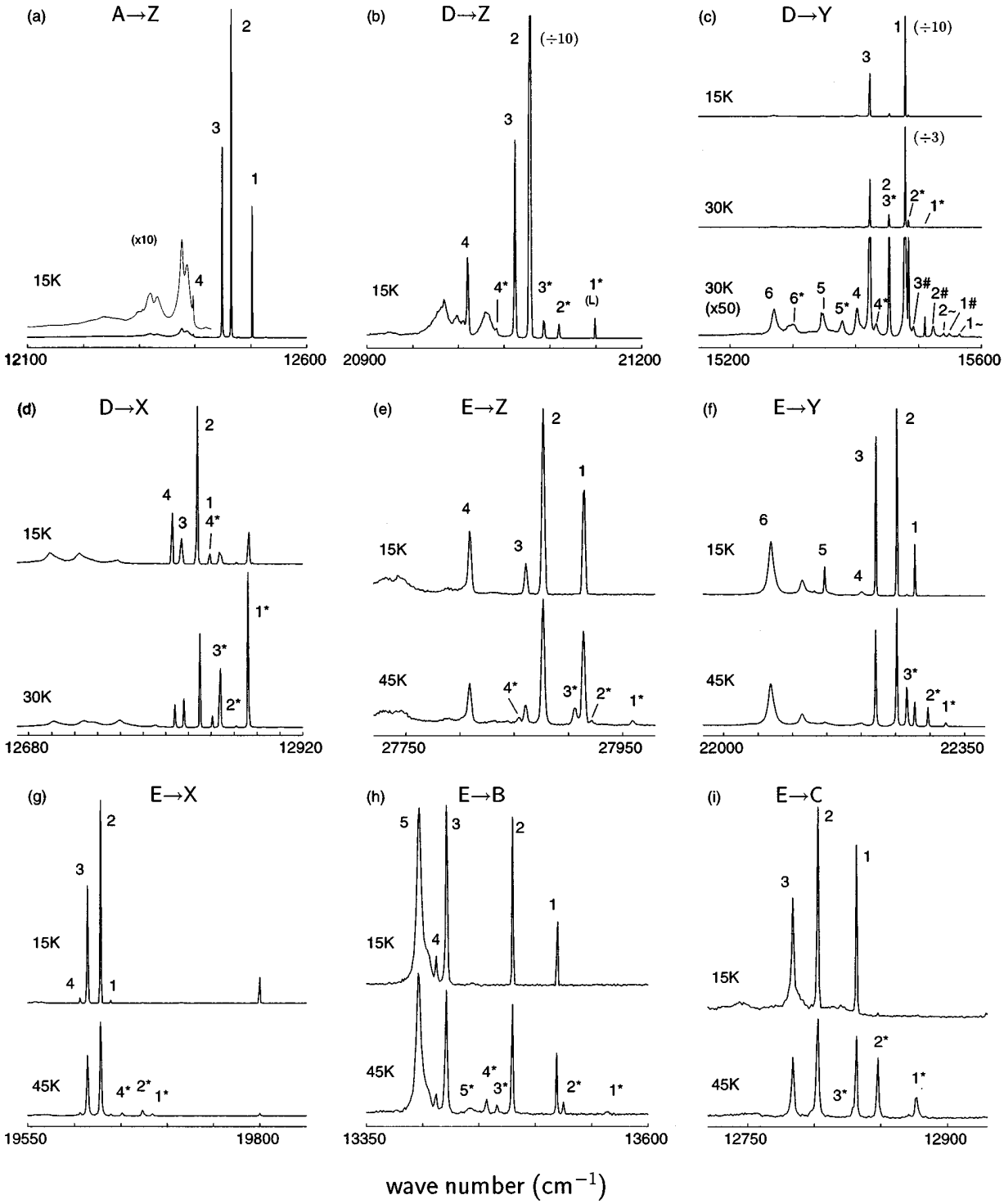

FIG. 5. Fluorescence spectra of the $C_{3v}(B)$ center in CaF_2:0.05%Tm^{3+} taken at the indicated temperatures. (a) $A \rightarrow Z$ transitions, pumping $Z_1 \rightarrow B_3$ at 14 497 cm^{-1}, (b), (c), (d) $D \rightarrow Z$, $D \rightarrow Y$ and $D \rightarrow X$ transitions, pumping $Z_1 \rightarrow D_2$ at 21 150 cm^{-1}, (e), (f), (g), (h), (i) $E \rightarrow Z$, $E \rightarrow Y$, $E \rightarrow X$, $E \rightarrow B$, and $E \rightarrow C$ transitions, pumping $A_1 \rightarrow E_2$ ESA at 15 462 cm^{-1}. Fluorescence transitions are labeled by numerical labels for energy levels of the lower multiplet, with transitions originating from the first, second, and third excited states of the upper multiplet denoted with $*$, #, and $\sim$, respectively.

C. Crystal-field calculations

In analyzing the energy level structure of the Tm^{3+} ion in these two centers, the free-ion and crystal-field Hamiltonian matrices for the entire $4f^{12}$ configuration were diagonalized simultaneously, thereby including all intermediate-coupling and crystal-field J-mixing effects. The free-ion Hamiltonian is parametrized as[13]

$$\mathcal{H}_f = \sum_{k=2,4,6} F^k f_k + \sum_i \zeta \boldsymbol{l}_i \cdot \boldsymbol{s}_i + \alpha L(L+1) + \beta G(G_2) + \gamma G(R_7) + \sum_{k=0,2,4} M^k m_k + \sum_{k=2,4,6} P^k p_k . \quad (1)$$

TABLE VII. Measured and calculated energy levels for the CaF_2:Tm^{3+} C_{3v} center. Irreducible representation assignments determined from the best crystal-field energy fit to assigned energy levels of the C_{3v} center.

Energy level		Energies (cm^{-1}) measured	calculated
$^3H_6$	γ_1	0.0	7.9
	γ_2	37.4	29.3
	γ_3	53.4	60.8
	γ_3	105.1	100.9
	γ_3	-	195.1
	γ_1	-	211.2
	γ_3	-	266.1
	γ_3	-	317.3
	γ_1	-	385.0
$^3F_4$	γ_1	5639.9	5634.7
	γ_3	5664.7	5658.1
	γ_3	5696.6	5700.5
	γ_2	5716.9	5717.4
	γ_1	5770.7	5770.9
	γ_3	5848.2	5855.6
$^3H_5$	γ_2	8279.6	8266.0
	γ_3	8290.2	8299.2
	γ_1	8304.0	8301.1
	γ_3	8312.2	8322.9
	γ_3	-	8394.1
	γ_2	-	8417.4
	γ_3	-	8460.2
$^3H_4$	γ_3	12501.5	12521.0
	γ_1	12564.6	12555.9
	γ_2	-	12604.7
	γ_3	-	12683.8
	γ_3	-	12768.9
	γ_1	-	12820.4
$^3F_3$	γ_2	14398.8	14411.7
	γ_3	14438.2	14432.6
	γ_1	14497.2	14487.2
	γ_2	14506.9	14500.6
	γ_3	14520.8	14523.0
$^3F_2$	γ_3	15086.2	15071.8
	γ_1	15115.7	15113.8
	γ_3	15134.0	15132.2
$^1G_4$	γ_1	21118.9	21108.8
	γ_3	21149.8	21145.7
	γ_3	21205.3	21210.0
	γ_2	21225.2	21231.4
	γ_1	-	21276.0
	γ_3	-	21428.8
$^1D_2$	γ_3	27918.4	27923.8
	γ_3	27963.1	27967.0
	γ_1	-	27996.4

The splitting of the $4f^{12}$ configuration into multiplets is dominated by the electrostatic and spin-orbit terms and the F^k and ζ parameters which represent these were varied freely in the fit. The remaining terms representing configuration interactions (α,β,γ), spin-spin and spin-other-orbit interactions (M^k), and two-body electrostatically correlated magnetic interactions (P^k) play a relatively small part. These terms were included, but were held fixed at values reported for LaF_3,[13] rather than being varied.

Because the immediate environment of the Tm^{3+} ion in both sites is approximately cubic, the terms in the C_{4v} and C_{3v} crystal-field Hamiltonians were grouped into terms which transform as specific irreducible representations of the O_h group. The respective crystal-field Hamiltonians used were

$$\begin{aligned}\mathcal{H}_{C_{4v}} = {} & B_C^4\left[C_0^{(4)} + \sqrt{\frac{5}{14}}\,(C_4^{(4)} + C_{-4}^{(4)})\right] \\ & + B_C^6\left[C_0^{(6)} - \sqrt{\frac{7}{2}}\,(C_4^{(6)} + C_{-4}^{(6)})\right] \\ & + B_A^2 C_0^{(2)} + B_A^4\left[C_0^{(4)} - \sqrt{\frac{7}{10}}\,(C_4^{(4)} + C_{-4}^{(4)})\right] \\ & + B_A^6\left[C_0^{(6)} + \sqrt{\frac{1}{14}}\,(C_4^{(6)} + C_{-4}^{(6)})\right], \end{aligned} \tag{2}$$

$$\begin{aligned}\mathcal{H}_{C_{3v}} = {} & B_C^4\left[C_0^{(4)} + \sqrt{\frac{10}{7}}\,(C_3^{(4)} - C_{-3}^{(4)})\right] \\ & + B_C^6\left[C_0^{(6)} - \sqrt{\frac{35}{96}}\,(C_3^{(6)} - C_{-3}^{(6)})\right. \\ & \left. + \sqrt{\frac{77}{192}}\,(C_6^{(6)} + C_{-6}^{(6)})\right] \\ & + B_A^2 C_0^{(2)} + B_A^4\left[C_0^{(4)} - \sqrt{\frac{7}{40}}\,(C_3^{(4)} - C_{-3}^{(4)})\right] \\ & + B_A^6\left[\sqrt{\frac{11}{42}}\,(C_3^{(6)} - C_{-3}^{(6)}) + \sqrt{\frac{5}{21}}\,(C_6^{(6)} + C_{-6}^{(6)})\right] \\ & + \hat{B}_A^6\left[C_0^{(6)} + \sqrt{\frac{160}{1029}}\,(C_3^{(6)} - C_{-3}^{(6)})\right. \\ & \left. - \sqrt{\frac{176}{1029}}\,(C_6^{(6)} + C_{-6}^{(6)})\right], \end{aligned} \tag{3}$$

where, in each case, the B_C^k terms alone form a cubic-symmetry Hamiltonian and the B_A^k terms represent the non-cubic distortions appropriate to the overall C_{4v} or C_{3v} symmetry.

One further parameter is required for each fit, representing a uniform shift of the entire configuration to bring the zero of energy to an appropriate level. The fitted parameters for the 31 levels of the C_{4v} center and the 30 levels of the C_{3v} center are listed in Tables VIII and IX, respectively.

For the C_{4v} center, the irreducible representations for the various energy levels were determined by the polarized LSE studies and used to assign energy levels for the crystal-field fit. A standard deviation of 8.3 cm^{-1} was obtained for the fit over 31 levels. From its assigned crystal-field wave function, the $g_\parallel$ value of the B_1 level was calculated to be $g_\parallel = 5.9$, in reasonable agreement with previous optical-Zeeman experiments which gave a g value of $g_\parallel = 6.1$.[14] The crystal-field

TABLE VIII. Best-fit values for the free-ion and crystal-field parameters (all in cm^{-1}) which were varied in the crystal-field fit for the C_{4v} center of CaF_2:Tm^{3+}. Remaining free-ion parameters were fixed at the values for LaF_3:Tm^{3+} (Ref. 13).

Parameter	Value (cm^{-1})	Parameter	Value (cm^{-1})
F^2	102249.9	B_A^2	567.0
F^4	71603.9	B_A^4	392.8
F^6	51401.8	B_A^6	385.5
ζ	2633.8	B_C^4	−1100.7
		B_C^6	489.0

parameters obtained are very similar to those reported for the C_{4v} centers in CaF_2:Er^{3+} (Ref. 15) and CaF_2:Ho^{3+} (Ref. 4), confirming that these centers are structurally similar.

For the C_{3v} center, irreducible representations for the various energy levels could not be unambiguously determined from the LSE spectra. Assignment of energy levels to particular crystal-field levels followed from an initial crystal-field calculation using estimated parameters. Following a fit from these assignments, two pairs of levels which had been reversed in order were reassigned to obtain the final fit. The assignment of the crystal-field levels were checked by repeating the fit with the exclusion of the levels of each multiplet in turn. The resulting predicted ordering and splitting of the multiplet in question was then compared with the experimental levels. In each case, the prediction was totally consistent with the assignments which had been made. A reasonable standard deviation of 10.2 cm^{-1} over the 30 measured levels was obtained. However, many of the proposed assignments are not consistent with the electric-dipole selection rules of Table V. Hence, the final level asssignments are tentative and are presented only as a basis for further investigations. Polarized LSE results performed with an applied magnetic field would help establish unambiguous irreducible representation identifications.

D. Fluorescence lifetimes

The fluorescence decay times for fluorescence from the lowest levels of the $^3H_4(A)$, $^1G_4(D)$, and $^1D_2(E)$ multiplets for the C_{4v} and C_{3v} centers in CaF_2:0.05%Tm^{3+} are given in Table X. No significant changes in these were observed for Tm^{3+} concentrations varying from 0.01% to 0.1%.

TABLE IX. Best-fit values for the free-ion and crystal-field parameters (all in cm^{-1}) which were varied in the crystal-field fit for the C_{3v} center of CaF_2:Tm^{3+}. Remaining free-ion parameters were fixed at the values for LaF_3:Tm^{3+} (Ref. 13).

Parameter	Value	Parameter	Value
F^2	102372.0	B_A^2	231.4
F^4	71469.8	B_A^4	374.4
F^6	51497.8	$\hat{B}_A^6$	−480.9
ζ	2635.6	B_A^6	−411.3
		B_C^4	−40.7
		B_C^6	556.5

TABLE X. Measured fluorscence lifetimes (in ms, ±5%) of the $^3H_4$, $^1G_4$, and $^1D_2$ multiplets for the C_{4v} and C_{3v} centers of CaF_2:Tm^{3+}.

	CaF_2:Tm^{3+} lifetime	
Multiplet	C_{4v} center	C_{3v} center
$^3H_4$	3.3	3.1
$^1G_4$	2.1	1.1
$^1D_2$	0.18	0.10

E. Temperature dependence of the upconversion fluorescence

We reported the phenomenon of upconversion fluorescence in CaF_2:Er^{3+} and CaF_2:Tm^{3+} achieved by pumping either GSA or ESA transitions with a single tunable laser.[5] In contrast to a report of upconversion observed in CaF_2:0.2%Tm^{3+},[16] the upconversion in our case is from single Tm^{3+} ion centers. It is caused by the overlap of a strong purely electronic ESA transition with weak vibronic sidebands associated with GSA transitions. Thus the laser is able to pump both transitions, one strongly and one weakly, at the same frequency.

It was found[5] that, for pumping the $Y_1 \rightarrow D_1$ transition of the C_{4v} center in CaF_2:Tm^{3+}, the upconversion fluorescence increased dramatically as the sample was warmed from 10 K, being enhanced by a factor of 100 at room temperature (Fig. 6). This is attributed to the $Y_1 \rightarrow D_1$ ESA transition at 15 344 cm^{-1} having a transition energy only 21 cm^{-1} from the $Z_1 \rightarrow C_2$ GSA transition at 15 365 cm^{-1}. At low temperatures, there is essentially no overlap between these two electronic transitions, and the overlap with vibronic sidebands of lower-energy GSA transitions is responsible for the weak upconversion fluorescence observed. However, as the temperature increases, the two transitions broaden and begin to overlap, giving a much greater combined transition probability. In addition, the $Z_2 \rightarrow C_2$ GSA transition near 15 280 cm^{-1} has a much stronger transition moment than the $Z_1 \rightarrow C_2$ transition and becomes important once the Z_2 state acquires significant population at elevated temperatures.

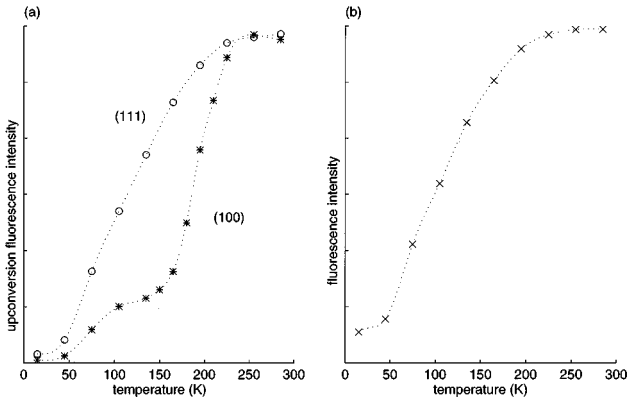

FIG. 6. Temperature dependence of the fluorescence intensity of the Tm^{3+} C_{4v} center for laser pumping at the $Y_1 \rightarrow D_1$ excitation line at 15 344 cm^{-1}. (a) $D \rightarrow Z$ upconversion blue fluorescence intensity monitored over a band of blue wavelengths for ⟨100⟩- and ⟨111⟩-oriented CaF_2:Tm^{3+}, and (b) $A \rightarrow Z$ infrared fluorescence intensity for ⟨111⟩-oriented CaF_2:Tm^{3+}.

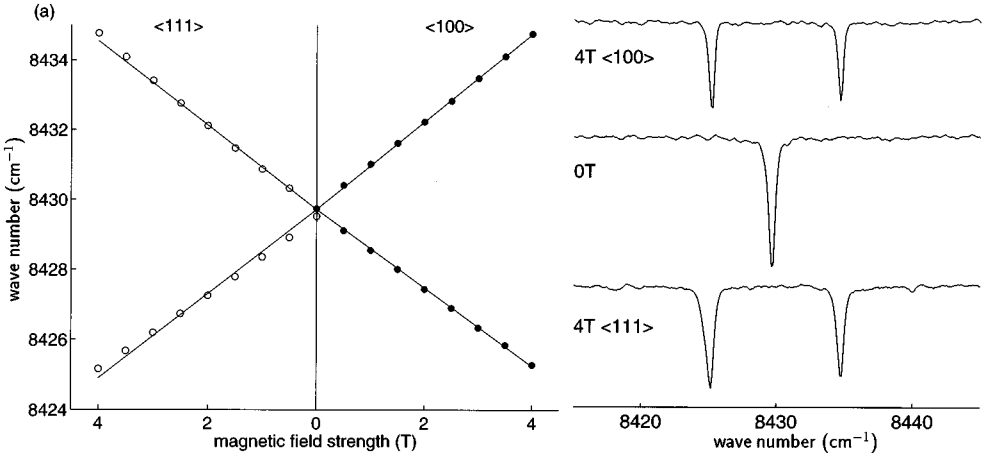

FIG. 7. Zeeman splittings of the $^3H_6 \rightarrow {}^3H_5$ absorption line of the cubic center. (a) Splitting diagram for magnetic fields applied parallel to the ⟨111⟩ and ⟨100⟩ crystal axes. (b) 4 T ⟨100⟩, zero field, and 4 T ⟨111⟩ absorption spectra of the cubic center transitions.

In Fig. 6(b), the temperature dependence of the $^3H_4 \rightarrow {}^3H_6$ usual fluorescence is shown, for laser pumping at the same $Y_1 \rightarrow D_1$ excitation frequency. This curve represents the ground-state absorption rate for pumping at that frequency, as nonradiative decay to the $^3H_4$ multiplet is the predominant decay path for Tm^{3+} ions excited into the $^3F_3$ and $^3F_2$ multiplets. Curve (b) appears qualitatively similar to curve (a) for ⟨111⟩-oriented crystals, demonstrating that the efficiency of the off-resonance GSA step dominates the temperature dependence. For ⟨100⟩-oriented crystals, the temperature dependence of the $^3H_4 \rightarrow {}^3H_6$ normal fluorescence follows a similar shape to that for ⟨111⟩-oriented crystals. However, the shape of the upconversion-fluorescence curve has a significantly different shape, which is attributed to the second, ESA, step in the upconversion process.

This can be explained in terms of the strong polarization dependence of transitions for C_{4v} centers. For a ⟨100⟩-oriented sample, all $Tm^{3+}C_{4v}$ centers are oriented either parallel or perpendicular to the incident laser polarization direction and their transition intensities are dependent on the specific center orientation. As the ESA absorption is a $\gamma_3 \rightarrow \gamma_3$ π-allowed transition and π and σ transitions excite differently oriented C_{4v} centers independently, only overlap by GSA transitions of π polarization will contribute to assisting the ESA upconversion fluorescence. With a change in temperature, the set of nearby GSA levels will contribute a varying combination of σ and π transitions, which determines the upconversion fluorescence level.

For a ⟨111⟩-oriented sample, all C_{4v} centers are equally inclined at 54.7° to the incident laser polarization direction and the combined sequential absorption intensity is from equivalently oriented centers with no strong polarization dependence expected.

At temperatures above 160 K, C_{4v} centers start to freely reorient and spectral polarization effects wash out.[17] Hence, the temperature dependence of the upconversion becomes independent of the laser polarization at higher temperatures.

The upconversion fluorescence from the $^1D_2$ multiplet, measured for pumping the $A_1 \rightarrow E_1$ ESA transition at 15 518 cm^{-1}, increased with temperature only to 60 K, beyond which it began to decrease. As there are no electronic GSA transitions near this 15 518 cm^{-1} energy, this behavior is attributed to changing phonon-sideband intensities.

In contrast, for the C_{3v} center, the intensity of upconversion fluorescence from either the $^1G_4$ or the $^1D_2$ multiplet did not increase at all when the temperature was increased above 10 K.

F. Identification of a cubic center

In the infrared-absorption spectrum of the $^3H_5$ multiplet, Fig. 1(b), a strong absorption line (identified as O) was found at 8429.6 cm^{-1} which could not be attributed to either the C_{4v} or C_{3v} centers. As this line is the only unassigned strong absorption line for all of the excited multiplets up to $^1D_2$ at 30 000 cm^{-1} the possibility of it being associated with a Tm^{3+} cluster center could be rejected. This line is assigned to a Tm^{3+} center of cubic symmetry.

In external magnetic fields of up to 4 T, applied parallel to either the ⟨100⟩ or ⟨111⟩ crystal axes, this line was observed to split into two components. The spectra at 4 T in each orientation and the zero-field spectrum of this line are shown in Fig. 7(b), while Fig. 7(a) shows the experimental splitting diagrams with a superimposed linear fit to each.

The g values from these linear fits are

$$g_{\langle 100\rangle} = 5.09 \pm 0.10,$$

$$g_{\langle 111\rangle} = 5.17 \pm 0.10.$$

Within experimental uncertainty, the g value is isotropic, which supports the assignment of this line to a cubic-symmetry center.

Because this center has a center of inversion, electric-dipole transitions are strictly forbidden. Any observed pure electronic transitions of this cubic center could only be magnetic-dipole allowed. From the $\Delta J = 0, \pm 1$, $\Delta L = \Delta S = 0$ selection rules for magnetic-dipole transitions, only the $^3H_6 \rightarrow {}^3H_5$ transitions of Tm^{3+} are allowed in magnetic-dipole absorption. This accounts for the absence of cubic center transitions in the absorption spectra to other multiplets.

The cubic crystal-field Hamiltonian for the $4f^n$ configuration is parametrized by two parameters B_C^4 and B_C^6:

$$\mathcal{H} = B_C^4 C_C^{(4)} + B_C^6 C_C^{(6)}.$$

The form of the angular operators of the fourth and sixth degree cubic terms, $C_C^{(4)}$ and $C_C^{(6)}$, are given by the leading two terms of Eq. (2) or (3), depending on whether tetragonal or trigonal quantization axes are chosen. Plots of the cubic crystal-field eigenvalues for all J manifolds as a function of the cubic crystal field for the tetragonal quantization basis have been published.[18] These give the cubic-field energies as a function of the admixture X of the fourth and sixth degree terms of the cubic crystal-field Hamiltonian.

Estimates for the cubic crystal-field parameters can be obtained by considering the parameters found for the cubic center in CaF_2:Er^{3+}, (Ref. 8) or by taking the cubic part of the C_{4v} symmetry Hamiltonian for CaF_2:Tm^{3+} C_{4v} center. In either case, the $J=6$ splitting diagram[18] shows that the ground state of Tm^{3+} in this cubic center has a cubic irreducible representation of Γ_2. This cubic irreducible representation decomposes to γ_3 in C_{4v} symmetry, in agreement with the γ_3 ground state adopted for the C_{4v} center. As the magnetic-dipole operator transforms as Γ_4, transitions from the ground state are allowed only to $\Gamma_4 \otimes \Gamma_2 = \Gamma_5$ states. There is only one Γ_5 state in the $^3H_5(X)$ multiplet, consistent with the observation of only one transition for the cubic center. The $J=5$ splitting diagram[18] shows this Γ_5 state to be to the lowest (X_1) level of the $^3H_5$ multiplet.

As the $^3H_6(\Gamma_2)$ initial and $^3H_5(\Gamma_5)$ final states are the only Γ_2 and Γ_5 states of their respective multiplets, their wave functions are independent of the crystal-field parameters and are given by group theoretical considerations. For the tetragonal quantization axis these wave functions are

$$|Z_1, {}^3H_6, \Gamma_2\rangle = \sqrt{\frac{11}{32}}\,(|{}^3H_6, 2\rangle + |{}^3H_6, -2\rangle) - \sqrt{\frac{5}{32}}\,(|{}^3H_6, 6\rangle + |{}^3H_6, -6\rangle)$$

$$|X_1, {}^3H_5, \Gamma_5\rangle = \begin{cases} \sqrt{\frac{15}{32}}\,|{}^3H_5, \pm 5\rangle - \sqrt{\frac{14}{32}}\,|{}^3H_5, \pm 1\rangle \\ \quad - \sqrt{\frac{3}{32}}\,|{}^3H_5, \mp 3\rangle, \\ \frac{1}{\sqrt{2}}(|{}^3H_5, 2\rangle + |{}^3H_5, -2\rangle) \end{cases}.$$

In a magnetic field applied along either the tetragonal or trigonal quantization axis, the Γ_5 triplet splits into three levels having magnetic-dipole σ_R, π, and σ_L absorption transitions from the unsplit Γ_2 ground state. In the experimental arrangement used the light propagation axis is necessarily parallel to the applied magnetic-field axis so that π transitions cannot be observed, leaving two subtransitions as observed. The isotropic g value calculated from this wave function is

$$g = 5.17,$$

which is in excellent agreement with the measured g values, confirming the assignment of this center to the cubic center.

G. Relative concentrations of cubic and C_{4v} centers

In principle, the concentration N of a particular center in a crystal can be found from the integrated absorption coefficient of an absorption line and the oscillator strength of that transition. In the absorption spectrum of the $^3H_5$ multiplet for CaF_2:Tm^{3+} we have one transition $Z_1 \rightarrow X_1$ for each of the cubic and C_{4v} centers, which is purely magnetic-dipole in character. Unlike electric-dipole transitions, magnetic-dipole transition strengths can be readily calculated if the JM-basis wave functions of the initial and final states are known.

The Z_1 and X_1 wave functions of the cubic center have been given in Sec. III F, and the corresponding wave functions of the C_{4v} center can be calculated from the crystal-field fit performed in Sec. III C and are

$$|Z_1, {}^3H_6, \Gamma_2\gamma_3\rangle = 0.6991(|{}^3H_6, 2\rangle + |{}^3H_6, -2\rangle) - 0.1005(|{}^3H_6, 6\rangle + {}^3H_6, -6\rangle),$$

$$|X_1, {}^3H_5, \Gamma_5\gamma_4\rangle = 0.7063(|{}^3H_5, 2\rangle + |{}^3H_5, -2\rangle).$$

The matrix elements of the magnetic-dipole transition operator $\mathbf{L}+2\mathbf{S}$ between the Z_1 ground level and the X_1 upper level are calculated for both the cubic and the C_{4v} center. With averaging over the three components of the dipole operator for the cubic center transition and over the three possible orientations of the tetragonal axis for the C_{4v} center, matrix elements of 0.277 and 0.134 are obtained for the cubic and C_{4v} centers, respectively. The relative concentrations of these two centers are determined from their absorption line strengths. Assuming Lorentzian line shapes for the two transitions in the absorption spectrum of Fig. 7(b) for CaF_2:0.01%Tm^{3+}, the line strengths (integrated absorption coefficients) are 13.3 and 17.3 $cm^{-1}\,m^{-1}$ for the cubic and C_{4v} center lines, respectively.

These experimental line strengths and the calculated transition moments are combined to give a relative concentration of

$$\frac{N(C_{4v})}{N(\text{cubic})} = 2.7,$$

which may be compared with results described for CaF_2:Er^{3+}.[9] For 0.1% Er^{3+} the concentration of cubic centers is almost twice that of C_{4v} centers, but for 0.015% Er^{3+} the situation is reversed and the C_{4v} center concentration is about 1.5 times the cubic center concentration. These results are based on theoretical predictions and indirect estimates of the cubic center concentration from the total Er^{3+} concentration.

As the Tm^{3+} concentration is nominally 0.01% for the absorption spectrum analyzed, our result agrees with the CaF_2:Er^{3+} 0.015% findings. For higher Tm^{3+} concentrations up to 0.05%, the relative concentration of cubic centers increases, but the ratio achieved was found to be more a function of the crystal growth rate rather than the Tm^{3+} concentration.

The usefulness of the Tm^{3+} estimates is that they do not rely on any model of defect aggregration in CaF_2, but follow directly from measurements of relative line strengths and known crystal-field wave functions.

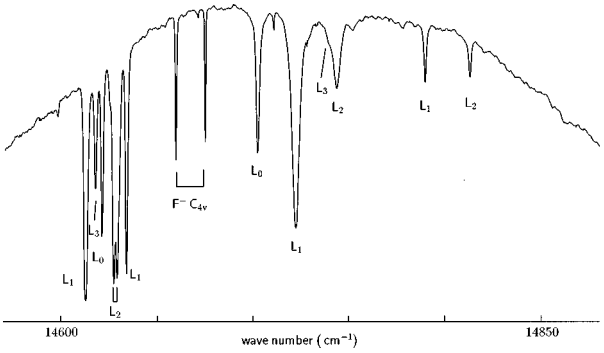

FIG. 8. 10 K laser transmission spectrum of the $^3F_6$ multiplet for deuterated CaF_2:0.05%Tm^{3+}. The new D^- centers are labeled L_0–L_3. The maximum absorption is 99.5% for the 10 mm sample length used.

H. D^--modified centers produced by deuteration of CaF_2:Tm^{3+}

The introduction of deuteride (D^-) ions into rare-earth-doped CaF_2 crystals produces a large number of new rare-earth centers involving the substitution of D^- ions for interstitial or lattice F^- ions.[1–3,19] Several new absorption features appeared in the $^3F_3$ multiplet absorption spectrum of CaF_2:Tm^{3+} and were grouped into two regions, one group near the F^- C_{4v} center absorption lines around 14 700 cm^{-1} and the other group near the F^-C_{3v} center absorption lines around 14 400 cm^{-1}.

As the lower-energy group of lines was beyond the tuning range of the rhodamine 640 dye laser, they were not studied further. They are believed to be D^--modified C_{3v} centers analogous to the P, L, T, N, S, and V centers found in CaF_2:Er^{3+}. The higher-energy group of lines, which appeared first at the lower D^- concentrations, was studied by LSE. Figure 8 shows the absorption spectrum of the $^3F_3$ multiplet for this group of lines in deuterated CaF_2:0.05%Tm^{3+}, obtained by measuring transmitted laser light. The new absorption features are assigned by LSE to four centers, labelled L_0–L_3. The $^3H_6(Z)\rightarrow{}^3F_3(B)$ excitation and $^3H_4(A)\rightarrow{}^3H_6(Z)$ fluorescence transitions measured for each of these centers are summarized in Table XI.

These absorption features resemble the modified D^-C_{4v} centers observed for CaF_2:Pr^{3+}:D^-, (Ref. 19), and this is supported by the polarization and bleaching behavior of these centers. The L_1, L_2, and L_3 centers all exhibit reversible polarized bleaching, similar to that previously observed for other rare earths.[1–3,19] From a D^- concentration series study, the L_0 center forms earliest, followed by the L_1 center. From its being the first center formed and from the absence of any bleaching behavior, the L_0 center is assigned as the D^- analog of the C_{4v} center with just a charge-compensating D^- ion located in the nearest-neighbor interstital position. The L_1, L_2, and L_3 centers then follow as the first three members of a series analogous to the five CS centers identified for CaF_2:Pr^{3+}. Of these, the L_1 center is believed to correspond to the the $CS(1)$ center involving one interstitial and one substitutional D^- ion.

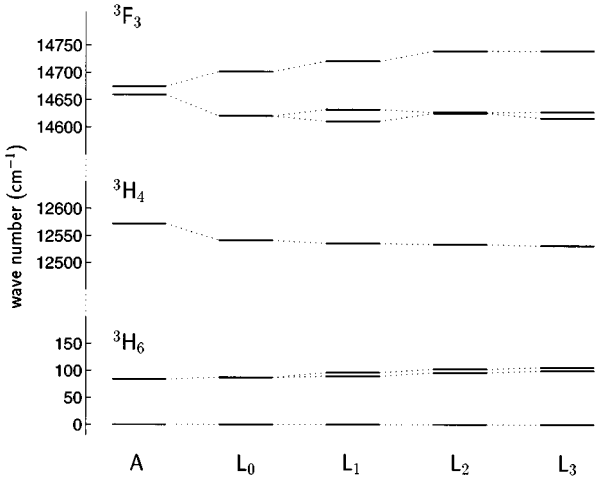

FIG. 9. Energy-level trends from the $F^-C_{4v}(A)$ center to the hydrogenic centers (L_0–L_3).

The $^3H_4(1)\rightarrow{}^3H_6(1)$ transition to the ground state is a γ_3 singlet to γ_3 singlet transition whose energy is relatively insensitive to the crystal field. For the L_0 to L_3 centers, this transition follows a systematic trend (Fig. 9 and Table II) to lower energies. This is the covalent shift from the successive replacement of F^- ions by D^- ions. First the charge-compensating F^- ion is replaced by a charge-compensating D^- with a shift from 12 571.9 to 12 541.4 cm^{-1}. Then there is a successive replacement of the four F^- ions between the Tm^{3+} ion and its charge compensating D^- ion.

The parent C_{4v} center has a γ_3 singlet ground state and a γ_5 doublet ground state 84 cm^{-1} above. With the L_0 center assigned as the D^-C_{4v} center, the same γ_3 singlet ground state is expected, and the first excited level of γ_5 symmetry is 87.4 cm^{-1} above. The L_1, L_2, and L_3 centers all have lower than C_{4v} symmetry as their first excited state of γ_5 symmetry is now split into sets of two closely spaced levels (Fig. 9 and Table XI). The similar splittings of about 6 cm^{-1} of these two levels indicate similar placements of the perturbing D^- off-axis neighbors in these three centers.

The crystal-field changes between the centers is evident in their absorption transition patterns, which differ markedly

TABLE XI. Transition energies (in cm^{-1}) of the $^3H_6\rightarrow{}^3F_3$ excitation and $^3H_4\rightarrow{}^3H_6$ fluorescence transitions of the L_0 to L_3 centers in deuterated CaF_2:Tm^{3+}.

	$^3H_6\rightarrow{}^3F_3$ excitation				$^3H_4\rightarrow{}^3H_6$ fluorescence		
Center	$\gamma_3\rightarrow\gamma_5$		$\gamma_3\rightarrow\gamma_3$	$\gamma_3\rightarrow\gamma_2$	$\gamma_3\rightarrow\gamma_5$		$\gamma_3\rightarrow\gamma_3$
L_0	14620.3		14701.4	-	12454.0		12541.4
L_1	14610.7	14632.2	14720.6	14788.5	12439.2	12446.1	12535.6
L_2	14625.6	14627.1	14739.4	14810.1	12431.0	12437.5	12533.9
L_3	14616.4	14627.8	14739.5	-	12425.4	12431.7	12531.4

(Fig. 9). The parent C_{4v} center has two sharp absorption transitions to the two lowest levels of γ_5 and γ_3 symmetry of the $^3F_3$ multiplet, which are separated by 15.3 cm^{-1} and weaker absorpton lines to higher levels of this multiplet (not included in Fig. 9). The small splitting of 15.3 cm^{-1} is from a partial cancellation between different-rank terms of the C_{4v} crystal field.

For the $D^- C_{4v}$ or L_0 center these two lowest levels are 81.1 cm^{-1} apart, which is attributed to different proportions of the different rank crystal-field terms for the D^- charge-compensated center, with much less cancellation.

For the lower-symmetry L_1–L_3 centers, the lowest γ_5 level of the $^3F_3$ multiplet is split into two components just as was discussed for the lowest γ_5 level of the ground $^3H_6$ multiplet. The L_1 center has these component levels separated by 21.5 cm^{-1}, the L_2 center by 1.5 cm^{-1}, and the L_3 center by 11.4 cm^{-1}.

The γ_3 second level of the $^3F_3$ multiplet follows a monotonic trend from 14 674.7 to 14 739.4 cm^{-1} (Fig. 9) as the crystal-field separation of the γ_5 and γ_3 levels of the $^3F_3$ multiplet increases along the L_0 to L_3 center sequence.

IV. CONCLUSIONS

Three single-Tm^{3+}-ion centers have been identified in CaF_2:Tm^{3+}. Two of these centers were identified using laser-selective excitation and upconversion techniques to have C_{4v} and C_{3v} symmetries, as for the principal and secondary centers found for CaF_2:Er^{3+} (Refs. 1 and 15) and CaF_2:Ho^{3+} (Ref. 4). Irreducible representations of the energy levels of the C_{4v} center were determined by polarization dependences and used to assign states for a crystal-field fit.

A third center was identified as a cubic-symmetry center from its single strong absorption line in the $^3H_5$ absorption spectrum. The isotropic Zeeman splittings of this line agree quantitatively with the magnetic behavior predicted by a cubic crystal-field analysis. Comparison of the line strength of this one cubic center absorption line with that of a related purely magnetic-dipole-allowed transition of the C_{4v} center allowed direct determination of the relative Tm^{3+} center concentrations. This method should find application for concentration series studies of Tm^{3+}, Eu^{3+}, and other centers for which pure magnetic-dipole transitions exist.

Tm^{3+} centers produced by deuteration are classified into D^--modified C_{4v} and D^--modified C_{3v} centers.

ACKNOWLEDGMENTS

This research was supported by the University of Canterbury and the New Zealand Lottery Board through research grants. We wish to thank M. F. Reid for making available his *f-Shell Empirical* crystal-field fitting routines, and R. J. Culley, R. A. Ritchie, and W. G. Smith for technical assistance.

*Present address: Department of Physics, Montana State University, Bozeman, Montana 59717.

[1] N. J. Cockroft, D. Thompson, G. D. Jones, and R. W. G. Syme, J. Chem. Phys. **86**, 521 (1987).
[2] R. J. Reeves, G. D. Jones, and R. W. G. Syme, Phys. Rev. B **46**, 5939 (1992).
[3] T. P. J. Han, G. D. Jones, and R. W. G. Syme, Phys. Rev. B **47**, 14 706 (1993).
[4] M. Mujaji, G. D. Jones, and R. W. G. Syme, Phys. Rev. B **46**, 14 398 (1992).
[5] N. M. Strickland and G. D. Jones, J. Lumin. **66&67**, 198 (1995).
[6] D. R. Tallant and J. C. Wright, J. Chem. Phys. **63**, 2074 (1975).
[7] C. W. Rector, B. C. Pandey, and H. W. Moos, J. Chem. Phys. **45**, 171 (1966).
[8] I. B. Aizenberg, B. Z. Malkin, and A. L. Stolov, Sov. Phys. Solid State **13**, 2155 (1972).
[9] D. S. Moore, Ph.D. thesis, University of Wisconsin, Madison, WI 1980;D. S. Moore and J. C. Wright, J. Chem. Phys. **74**, 1626 (1981).
[10] G. F. Koster, J. O. Dimmock, R. G. Wheeler, and H. Statz, *Properties of the Thirty-two Point Groups* (MIT Press, Cambridge, MA, 1963).
[11] M. F. Reid and P. H. Butler, J. Phys. C **15**, 4103 (1982).
[12] R. M. Macfarlane, Opt. Lett. **18**, 829 (1993).
[13] W. T. Carnall, G. L. Goodman, K. Rajnak, and R. S. Rana (unpublished).
[14] K. Muto, J. Phys. Chem. Solids **34**, 2029 (1972).
[15] C. A. Freeth, G. D. Jones, and R. W. G. Syme, J. Phys. C **15**, 5667 (1982).
[16] J. P. Jouart, M. Bouffard, G. Klein, and G. Mary, J. Lumin. **60&61**, 93 (1994).
[17] S. P. Jamison and R. J. Reeves, J. Lumin. **66&67**, 169 (1995).
[18] K. R. Lea, M. J. M. Leask, and W. P. Wolf, J. Phys. Chem. Solids **23**, 1381 (1962).
[19] R. J. Reeves, K. M. Murdoch, and G. D. Jones, J. Lumin. **66&67**, 136 (1995).